Surface & Coatings Technology 373 (2019) 65–74

Contents lists available at ScienceDirect

Surface & Coatings Technology

journal homepage: www.elsevier.com/locate/surfcoat

In-situ synthesis of TiC-Al_2O_3 coating on copper surface

Fang Yang[a,*], Qian Qin[a], Tao Shi[b], Xin Lu[a], Cunguang Chen[a], Zhimeng Guo[a,*], Alex A. Volinsky[c]

[a] Institute for Advanced Materials and Technology, University of Science and Technology Beijing, Beijing 100083, China
[b] GRIPM Advanced Materials Co., Ltd, Beijing 101407, China
[c] Department of Mechanical Engineering, University of South Florida, Tampa, FL 33620, USA

ARTICLE INFO

Keywords:
Copper
TiC
Al_2O_3
Coating
Self-propagating high-temperature synthesis
Vacuum-expendable pattern casting

ABSTRACT

In-situ TiC-Al_2O_3 strengthening coating was applied on copper, using the vacuum-expendable pattern casting (VEPC) in combination with the self-propagating high-temperature synthesis (SHS) technology. Due to the high heat consumption, highly exothermic CuO-Al (CA) reaction was employed to guarantee 100% completion of the Ti—C reaction. Consequently, TiC- Al_2O_3 coating was obtained after the ignition of Ti-C-CuO-Al SHS system by molten copper. Here, the optimal CA content was 10 wt%. During the casting process, molten copper infiltrated into the SHS coating, resulting in the achievement of dense coating microstructure. The hardness and wear resistance were also significantly improved. The hardness value of copper matrix was only 40 HB, while that of the composite coating was up to 195 HB. The mass loss reduced from 7.98 g to 0.44 g at 40 N load. Besides, metallurgical bonding was obtained with an ideal bond strength of 293 MPa.

1. Introduction

Copper is widely applied in optics, electrical contacts and heat conduction due to its high electrical and thermal conductivity, in addition to good fatigue resistance [1–4]. However, low hardness and poor wear resistance still limit copper industrial applications [5,6]. Thus, there is an increased interest to improve copper surface properties by employing surface coatings [7]. Numerous methods have been developed to produce surface coatings on copper, including internal oxidation [8], chemical vapor deposition [9], electrodeposition [10], pack cementation [11], high velocity oxygen fuel (HVOF) spraying [12], laser cladding [13], infiltration and self-propagating high-temperature synthesis (SHS) [14]. Of these methods, the SHS technique is a novel process for producing surface coatings, also known as combustion synthesis. It has advantages of low energy consumption, favorable exothermic reaction, high product purity and short reaction time [15–17]. Once the SHS reaction is ignited, the combustion wave propagates through the entire reacting mixture completely converting the reactants into in-situ reinforcements, such as TiC, TiB_2, Al_2O_3, SiC, WC, etc. [18,19]. As a drawback, the final products synthesized by the SHS reaction are highly porous. In this case, a subsequent process, just like extrusion, hot pressing, must be combined with the SHS for densification [20]. However, it is difficult to apply these techniques with SHS process in industrialized production due to the high cost and complexity.

Vacuum expendable pattern casting (VEPC) has been regarded as a promising method for producing complex-shaped parts due to its flexible design, low cost of foam pattern, high precision of investment casting, and better filling ability [21–23]. Our earlier research has presented a novel technology combining the SHS and the VEPC to apply in-situ TiC coatings on copper matrix [24]. The SHS combined with the VEPC can be utilized for industrial production of in-situ hard ceramic coatings on metals. Due to the particularly high combustion temperature of the Ti—C SHS system, close to the melting point of Ti [25], Cu powder was mixed with Ti—C mixtures to ensure the ignition reliability of SHS reaction during the VEPC process. However, because of significant heat consumption caused by Cu powder, the “frozen” phenomenon of the SHS reaction occurred, resulting in the existence of residual C and the formation of the Cu-Ti-C metastable phase. To solve this problem, the proper promoter may be added to the Ti—C system to replace the Cu powder.

Therefore, it is of interest to employ CuO-Al in the Ti—C SHS system to achieve the synthesis of in-situ TiC-Al_2O_3 composite coatings on copper matrix. First, CuO-Al SHS is a highly exothermic reaction with low activation energy barrier [26]. Besides, Al_2O_3 is a typical hard ceramic with ideal hardness and wear resistance [27,28]. So far, no related studies have been reported on the subject. In this paper, in-situ TiC-Al_2O_3 composite coating was obtained with a simultaneous copper cast. The reaction mechanism, microstructure, and mechanical properties of surface coatings were also investigated.

* Corresponding authors.
E-mail addresses: yangfang@ustb.edu.cn (F. Yang), zmguo@ustb.edu.cn (Z. Guo).

https://doi.org/10.1016/j.surfcoat.2019.05.064
Received 24 January 2019; Received in revised form 21 May 2019; Accepted 23 May 2019
Available online 26 May 2019

Table 1
The weight percent of each component in Ti-C-CuO-Al SHS system.

Sample	SHS system	Weight percent (wt.%)				CA content (wt.%)
		Ti	C	CuO	Al	
A1	Ti-C-CuO-Al	76	19	4.08	0.92	5
A2	Ti-C-CuO-Al	72	18	8.16	1.84	10
A3	Ti-C-CuO-Al	68	17	12.24	2.76	15
A4	Ti-C-CuO-Al	64	16	16.32	3.68	20

2. Experimental procedure

2.1. Raw materials preparation

The matrix material was pure copper. The raw materials for composite coating were comprised of Ti (99.7% pure, ~45 μm), graphite (99.5% pure, ~10 μm), CuO (99.9% pure, ~20 μm), and Al (99.7% pure, ~30 μm) powders. Table 1 lists the weight percentages of each component. Thereinto, the total mixture of CuO and Al (further flagged as CA) was chosen as an auxiliary system for the SHS reaction. The powders of Ti, Al, C and CuO were mixed in a planetary centrifugal mixer at atmospheric pressure for 2 h. Then, the mixed powders were pressed by hydraulic press with a pressure of 160 MPa. The size of green compacts with the relative density of 70% was 40 mm × 40 mm × 4 mm and Φ 15 × 15 mm^2.

2.2. Casting process

A typical VEPC process was employed to prepare TiC-Al_2O_3 strengthening coating on the copper surface, as shown in Fig. 1. First, the green compacts were pasted onto the surface of expendable polystyrene (EPS) patterns with the dimension of 40 mm × 40 mm × 20 mm. After drying at 50 °C for 2 h, a fireproof coating was brushed on the surface. Then, the coated pattern was placed into the silica sands. When pure copper was melted at 1200 °C, molten copper was poured into the sprue gate under vacuum (−0.04 to −0.05 MPa). Last, in-situ TiC-Al_2O_3 composite coating was obtained with cast copper simultaneously after cooling.

2.3. Tests and characterization

Five samples for each test were prepared to ensure verifiable repeatability. Differential scanning calorimetry (DSC) analysis was carried out under Ar atmosphere using NETZSCH STA449, at a constant heating rate of 10 °C/min. X-ray diffraction (XRD, Shimadzu XRD-6000, Cu Kα target, 40 kV and 40 mA) was employed for phase analysis. Microstructure observation and element distribution were performed -using a field emission scanning electron microscope (FESEM, Zeiss Supra55). Phase characterization was analyzed by transmission electron microscopy (TEM, Tecnai G2 F30 S-TWIN) equipped with energy dispersive spectrometer (EDS, GENESIS) and selected area electron diffraction (SAED) patterns. Besides, an ion milling system was employed to prepare the TEM specimens. The hardness was measured by the DHB-3000 hardness testing machine at 2.452 kN for 30 s. The shearing test was implemented on the basis of the YS/T485-2005 standard to present the bonding strength between the coating and copper matrix. Wear resistance test was performed in dry conditions, using the pin-on-disc tribometer based on the weight loss under various loads of 10, 20, 30, 40 N with rotating disc speed of 1382 mm/s. The tribometer was consisted of a sample holder and a rotating disc with the 600 grit SiC sandpaper on the surface. These tests were conducted on samples with Φ10 mm × 15 mm size for 20 min.

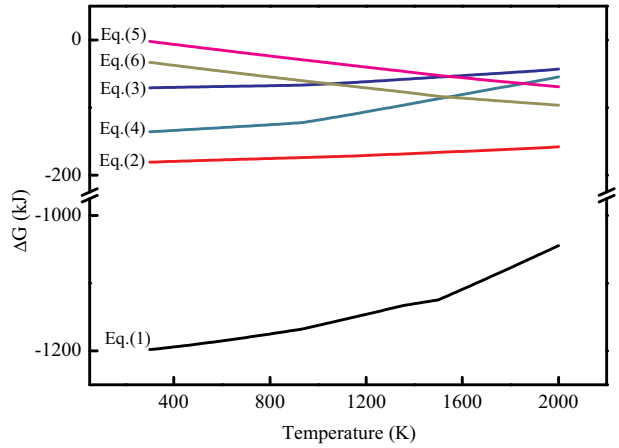

Fig. 2. Standard Gibbs free energy change curves as a function of temperature.

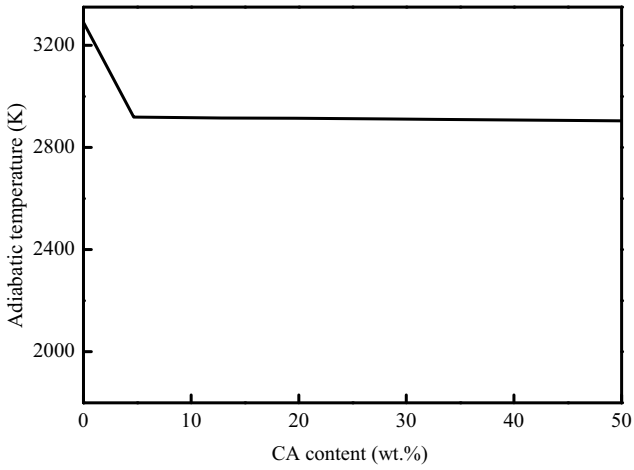

Fig. 3. Adiabatic temperature change of Ti-C-CA system with different CA amounts.

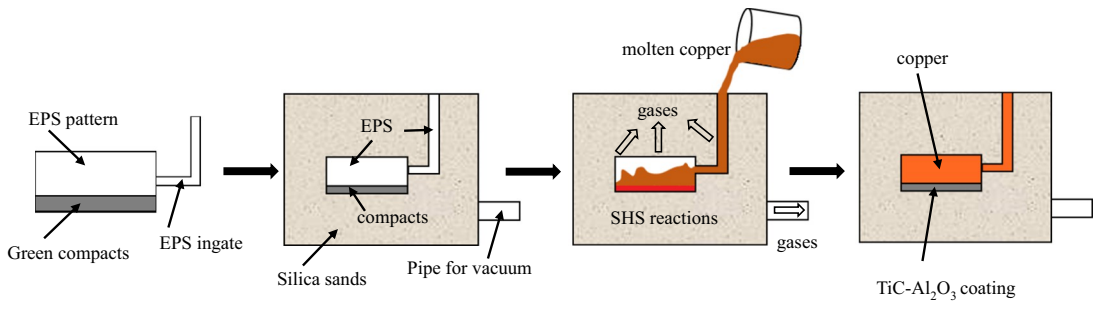

Fig. 1. Typical VEPC process for applying TiC-Al_2O_3 composite coating on copper surface.

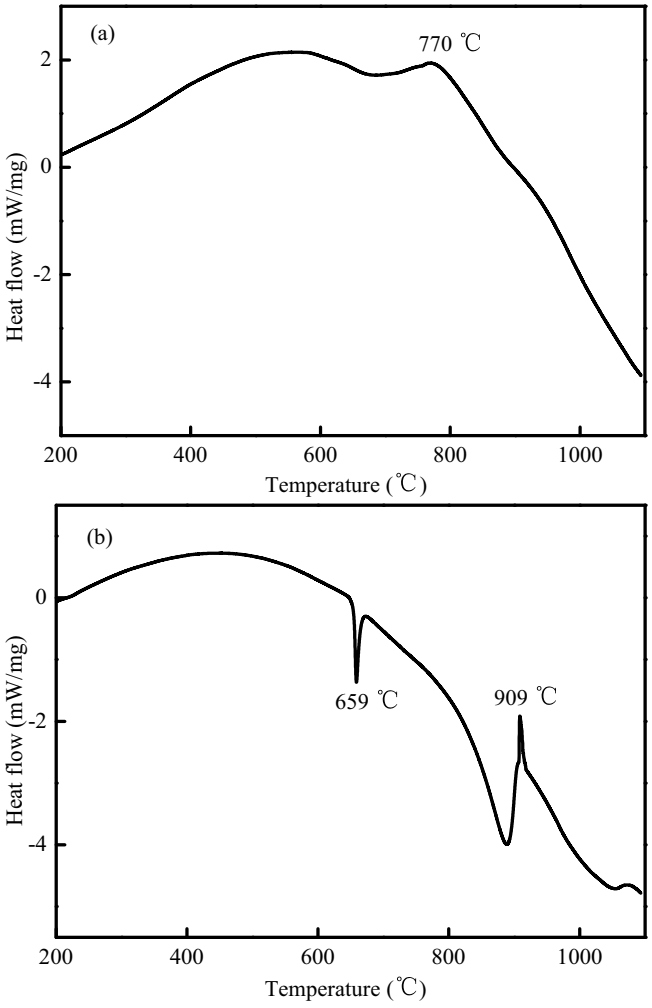

Fig. 4. DSC analysis of (a) Ti−C and (b) CuO-Al SHS systems.

3. Results and discussion

3.1. Reaction mechanism

For the sake of establishing the SHS reaction mechanism, the corresponding thermodynamics analysis of the Ti-C-CuO-Al system was performed. In light of the SHS system, the possible reactions are presented by Eqs. (1)–(6):

$$3CuO + 2Al \rightarrow 3Cu + Al_2O_3 \quad (1)$$

$$Ti + C \rightarrow TiC \quad (2)$$

$$Ti + Al \rightarrow TiAl \quad (3)$$

$$Ti + 3Al \rightarrow TiAl_3 \quad (4)$$

$$CuO + C \rightarrow Cu + CO \quad (5)$$

$$2CuO + C \rightarrow 2Cu + CO_2 \quad (6)$$

The corresponding Gibbs free energy (ΔG°) was theoretically calculated, as shown in Fig. 2. It can be observed that all reactions possess a negative ΔG°, indicating the thermodynamics feasibility of all above reactions during the copper casting process. Besides, the ΔG° for reaction (1) is much more negative than the other reactions. Therefore, it can be inferred that there was a higher tendency in the formation of the Cu and Al_2O_3 phases in the Ti-C-CuO-Al SHS reaction, followed by the formation of the TiC phase.

Whether the SHS reaction is self-sustaining depends on the adiabatic combustion temperature (T_{ad}) of the SHS reactive system. As reported in the literature [29], T_{ad} should be higher than 1800 K to induce its self-sustaining combustion synthesis process. For the Ti-C-CuO-Al system, the corresponding reaction can be written as:

$$Ti + C + n(3CuO + 2Al) \rightarrow TiC + n(3Cu + Al_2O_3) \quad (7)$$

Here, n is the CA molar quantity. In case the reaction conditions are adiabatic, the standard state enthalpy equilibrium equation can be balanced [30]:

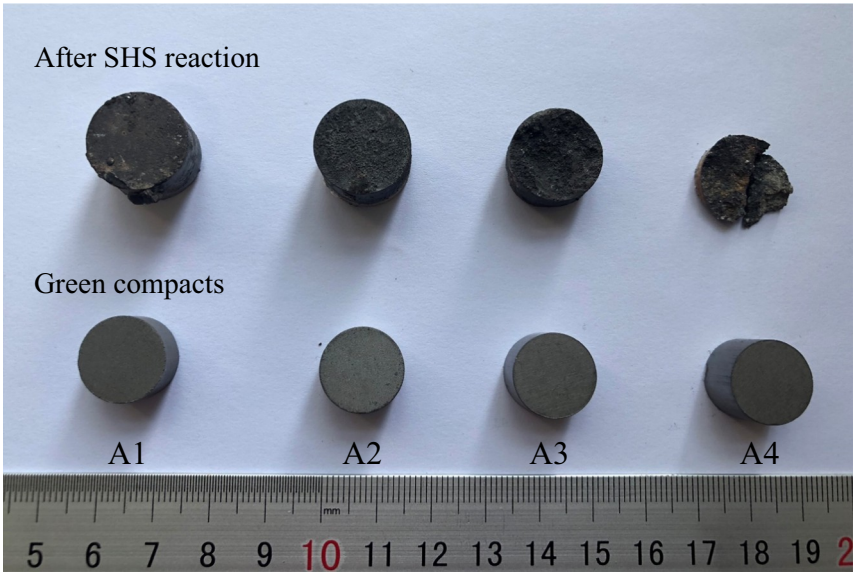

Fig. 5. Reaction status of Ti-C-CA SHS system with different CA amounts.

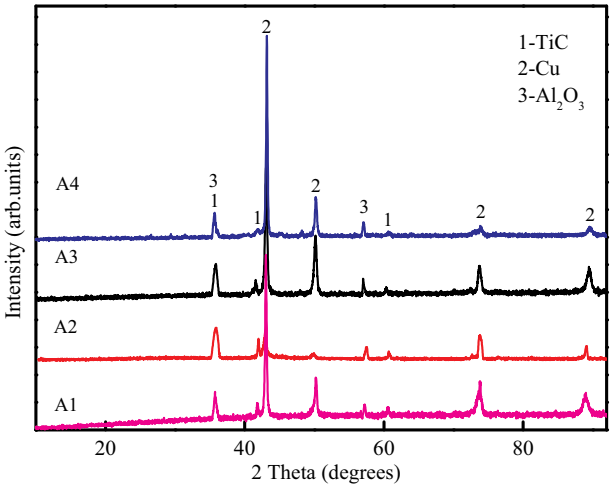

Fig. 6. XRD analysis of the SHS coatings in samples A1-A4.

$$\Delta H_{298}^{\theta} + \int_{298}^{Tad} \sum xC_Q(Q)dT + \sum_{298-T_{ad}} xH(Q) = 0 \quad (8)$$

where, $H_{298}{}^{\theta}$ corresponds to the standard state enthalpy at ambient temperature; x presents the number of moles; H(Q) and C_Q(Q) are the latent fusion heat and molar heat capacity, respectively.

In the light of the thermochemical data in reference [31], the T_{ad} value of Ti-C-CuO-Al system could be obtained according to reaction (9). Fig. 3 shows the corresponding T_{ad} curve as a function of the CA weight percent (w). Thereinto, w was determined by n, calculated as reaction (10). The T_{ad} value was far above 1800 K, indicating the Ti-C-CuO-Al SHS reaction was self-sustaining after being ignited. In addition, the T_{ad} value first reduced quickly with the CA addition and then reduced very slowly. When the CA SHS system was added in the Ti—C system, low melting point Al would melt first, resulting in heat consumption. In addition, Cu was formed after the CA SHS reaction. The melting and boiling points of Cu are about 1356 K and 2840 K, respectively. It can be deduced that reactant Cu would be transformed into a liquid, or even gas during the SHS process, and more heat would be absorbed. Therefore, the T_{ad} value of the Ti-C-CuO-Al system would be lower than the Ti—C system.

$$\Delta H_{f,298,TiC}^{\theta} + n\Delta H_{f,298,Al_2O_3}^{\theta} + n\Delta H_{f,298,Cu}^{\theta} + \int_{298}^{Tad} C_Q(TiC)dT + n \int_{298}^{Tad} C_Q(Al_2O_3)dT + n \int_{298}^{Tad} C_Q(Cu)dT + \sum_{298-T_{ad}} nH_x(Cu) = 0 \quad (9)$$

$$w = \frac{n(3M_{CuO} + 2M_{Al})}{M_{Ti} + M_C + n(3M_{CuO} + 2M_{Al})} \times 100 \quad (10)$$

DSC analysis for the Ti—C and CuO-Al system was performed to present the characteristic temperature of the thermal reaction, as presented in Fig. 4. The DSC test was conducted from ambient temperature to 1100 °C. Only one exothermic peak at 770 °C appeared in the Ti—C DSC curve. It can be inferred that the ignition temperature of the Ti—C SHS system may exceed 770 °C. There were two peaks observed in the CuO-Al DSC curve. The first endothermic peak at 659 °C was corresponding to the melting point of the Al phase, while the second

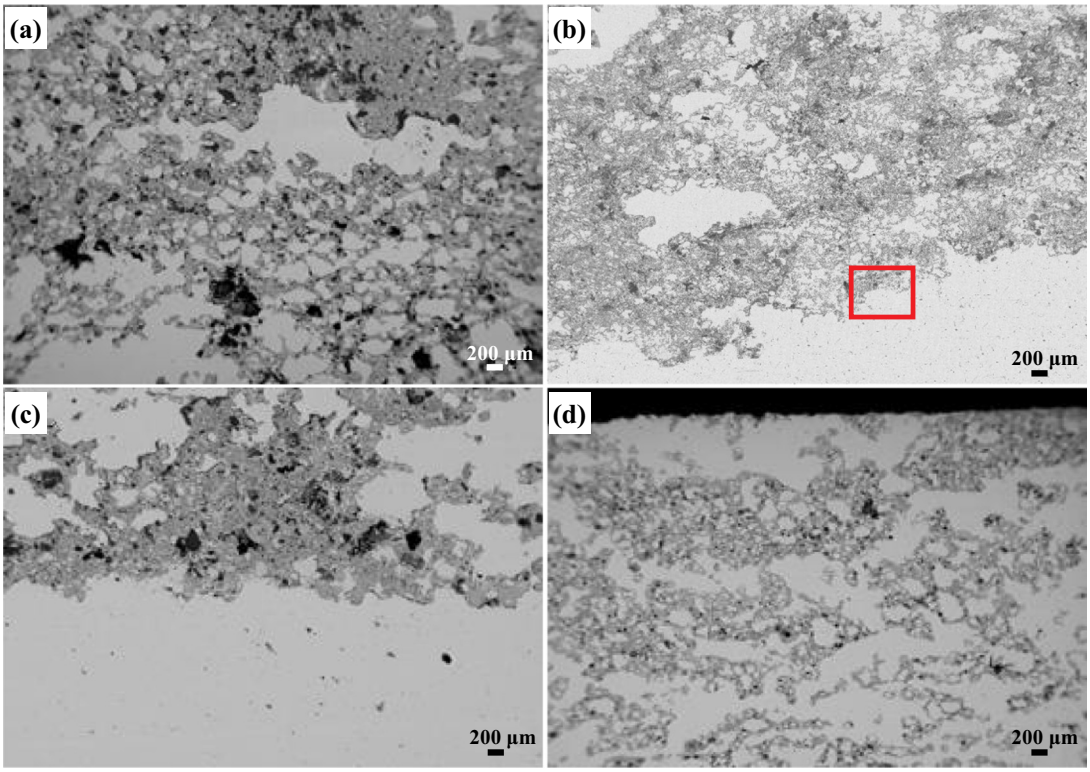

Fig. 7. Microstructure morphologies of the cross section of different samples: (a) A1, (b) A2, (c) A3, and (d) A4.

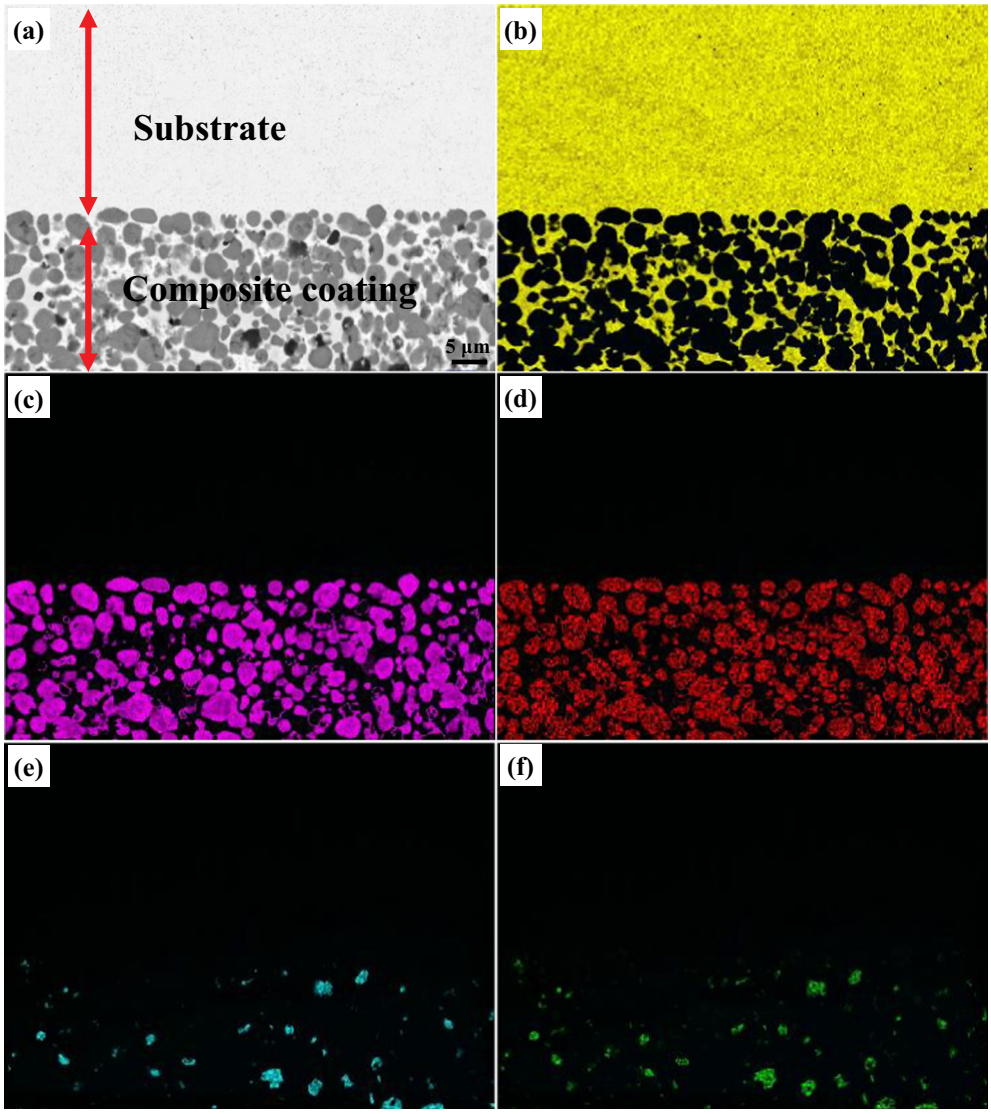

Fig. 8. (a) FESEM image of sample A2, and element distribution of: (b) Cu, (c) Ti, (d) C, (e) Al, and (f) O.

exothermic peak corresponded to the CuO-Al reaction temperature of 909 °C. It can be inferred that the temperature and heat of molten copper were high enough for igniting the Ti-C-CA SHS reaction.

To further confirm whether the Ti-C-CA SHS reaction can be ignited during the copper casting process, the comparison tests were conducted. When the sintering temperature reached 1200 °C, the green compacts (Φ 15 × 15 mm^2) were placed in the muffle furnace for 10 min with leaving the oven door open. Thus, the state of the SHS reaction could be easily observed. Fig. 5 presents the reaction status of the Ti-C-CA SHS system with different CA amounts. Due to the samples A1-A4 exposed to air without a protective atmosphere, the surface quality of the samples was poor due to oxidation. However, it was a remarkable fact that all SHS reactions were ignited at 1200 °C. With increasing CA content, the explosion of compacts was observed, especially in the A4 sample. It may be attributed to two reasons: one was the CuO decomposition, resulting in the production of a larger amount of gas, and another was the increase of reaction intensity.

3.2. Microstructure and phase identification

XRD analysis was carried out to confirm the coating phases, as shown in Fig. 6. TiC, Al_2O_3, and Cu phases were detected in the samples A1-A4. It can be deduced that the Ti-C-CA SHS reaction had been ignited during the casting process, resulting in the formation of TiC-Al_2O_3 composite coatings on the Cu matrix. There was no C peak observed, indicating that the Ti—C SHS reaction had been fully completed. As reported in Ref. [24], there was residual C observed in the composite coatings after the SHS reaction. The reactions of Ti—C or Ti-Cu-C were not fully completed. Due to a good thermal conductivity of Cu and heat consumption caused by Cu powder, the SHS reaction was partially "frozen". However, when the highly exothermic CA auxiliary system was added in the Ti—C system, the heat caused by the CA SHS reaction significantly promoted the Ti—C SHS reaction. During the casting process, once the molten copper touched the green compacts, the Ti—C SHS reaction was first ignited followed by the CA reaction in terms of the

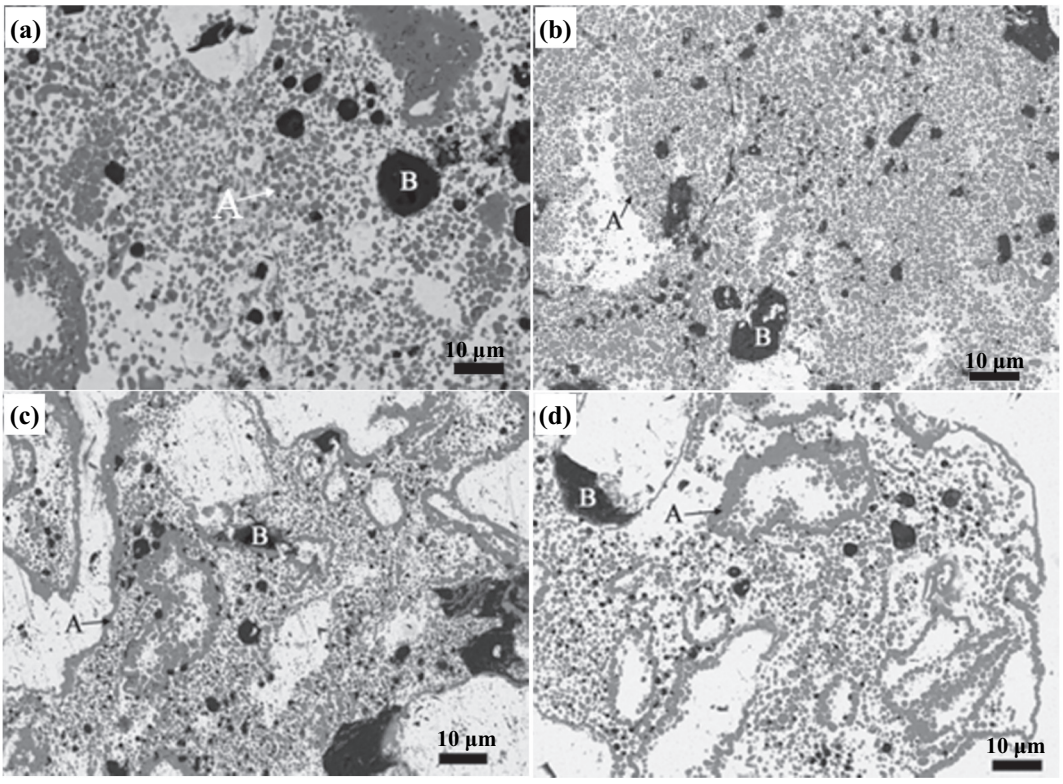

Fig. 9. SEM images of coating surface in sample: (a) A1, (b) A2, (c) A3, and (d) A4.

Table 2
Composition of region A and B in Fig. 9(a–d) determined by EDS analysis.

Element	Sample/wt.%							
	A1		A2		A3		A4	
	A	B	A	B	A	B	A	B
C	28	–	29	–	25	–	23	–
Ti	72	–	71	–	75	–	77	–
Al	–	60	–	55	–	58	–	56
O	–	40	–	45	–	42	–	44

The accuracy of EDS is +/− 1 wt.%.

DSC analysis. The CA reaction rate was very fast, while that of the Ti−C reaction was relatively slower. Due to adequate heat conductivity of Cu, the released heat produced by the CA reaction was enough to maintain the Ti−C SHS reaction.

Although the SHS synthesized products were porous, molten copper infiltrated into the composite coatings, resulting in the relatively dense microstructure, as shown in Fig. 7(b). When adding 10 wt% CA, the coating quality was relatively good with uniform microstructure. There were no apparent pores or defects observed. Besides, the metallurgically bonded coating was obtained. Except for the strengthening phase, the matrix phase was also observed in the coating microstructure. However, in the sample with 20 wt% CA addition, the coating homogeneity got worse and the composite coating debonded from the substrate. As shown in Fig. 5, the outgassing amount of the SHS system significantly increased with excessive CA introduction. Therefore, in terms of the coating microstructure, the optimal CA content for the TiC-Al_2O_3 composite coating is 10 wt%.

To indentify the interface characteristics between the coating and the copper matrix, the red region marked in Fig. 7(b) was observed at higher magnification. The corresponding element distributon analysis is presented in Fig. 8. Ti, Al, C, and O elements were obviously dominant in the coating layer. The C element completely overlapped with the Ti element, while the O element also completely overlapped with the Al element. From the XRD results, TiC and Al_2O_3 were the main coating phases. Note that the Cu element was also present in the coating except for matrix. Although Cu was formed after the CA reaction, the content was relatively low, about 6.5 wt% in the sample A2. Therefore, part of molten copper infiltrated into the SHS composite coatings, as shown in Fig. 7. Consequently, the metallurgically bonded coating was achieved.

Microstructure characteristics of the TiC-Al_2O_3 composite coating were further examined. The matrix phases corresponded to the light gray regions. Two kinds of strengthening phases (dark gray phase and black phase) were identified in Fig. 9. Combined with the EDS results in Table 2, the dark gray phase (spot “A”) was the TiC phase, while the black phase (spot “B”) was corresponding to the Al_2O_3 phase. Overall, a relatively uniform distribution of strengthening particles was observed in the sample A2. Fine TiC particles, nearly spherical, were formed. The particle size of Al_2O_3 was much larger than the TiC particles. Al_2O_3 was surrounded by the TiC phase, forming obvious clusters, as shown in Fig. 9. It can be also found that the trend of the coating being detached by molten copper was more and more apparent with the increasing CA content.

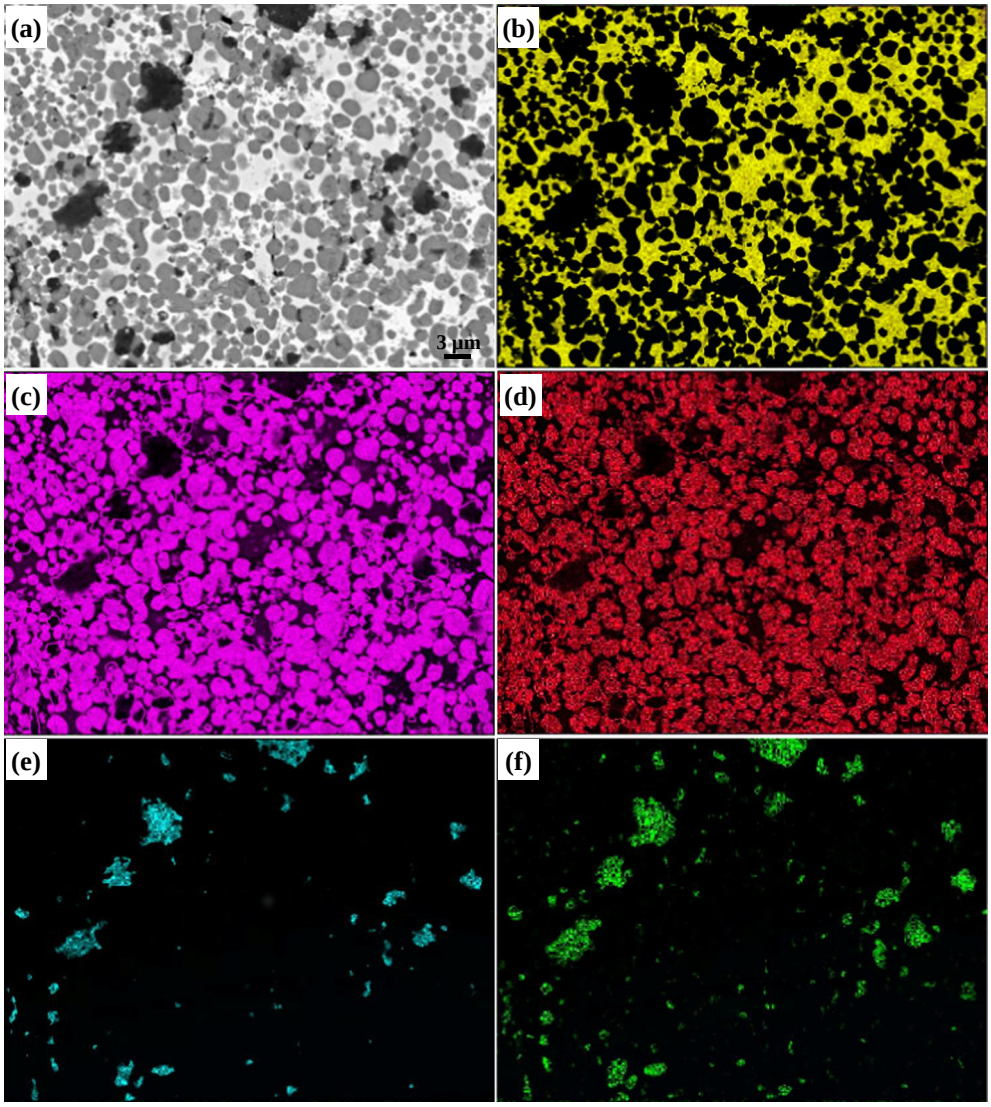

Fig. 10. (a) FESEM image of composite coating in sample A2, and element distribution of: (b) Cu, (c) Ti, (d) C, (e) Al, and (f) O.

In the sample A2, uniform and fine TiC particles were formed, about 1–3 μm, as seen in Fig. 10(a). The Ti−C SHS reaction was promoted by the CA SHS reaction, without residual C existence. Ti and C were mainly distributed in the dark gray region, and Al and O were mainly enriched in the black region. The differences in elemental distribution further indicated that the composite coating consisted of the TiC and Al_2O_3 phases. Besides, copper acted as a "binder", bonding the ceramic particles together with copper. Consequently, dense coating microstructure was obtained, as proven in Figs. 7–10. Thus, the bond strength between the matrix and the coating would be improved.

To identify the ceramic phase in the composite coating, TEM analysis was performed on sample A2. Thereinto, region "A" was the TiC phase with a cubic structure, as shown in Fig. 11(b). The measured distances from the (000) to (020), (200) planes were 0.211 nm and 0.213 nm, respectively. The corresponding zone axis was [001]. And, region "B" was the cubic Al_2O_3 phase with the lattice parameter of 0.795 nm. The corresponding measured distances were 0.447 nm and 0.240 nm, respectively. With the CA addition, the SHS reaction was fully completed, without the "frozen" effect reported in Ref. [24]. During the casting process, molten copper provided heat to ignite Ti−C and CuO-Al SHS reaction. The CA reaction rate was much higher, and the released heat produced by the CA system achieved thermal compensation for the Ti−C system.

3.3. Mechanical properties

Compared with the Cu matrix, the results shown in Fig. 12 indicated that the hardness values had been significantly increased within a measurement error of 5%. The hardness value of the Cu matrix was about 40 HB. The hardness increased first before decreasing with the CA content increasing. With the addition of 10 wt% CA, the hardness increased to 195 HB, reaching its maximum value. A hardness value enhancement of 388% was obtained. This might be associated with the uniform coating microstructure, as presented in Fig. 9(b). When adding

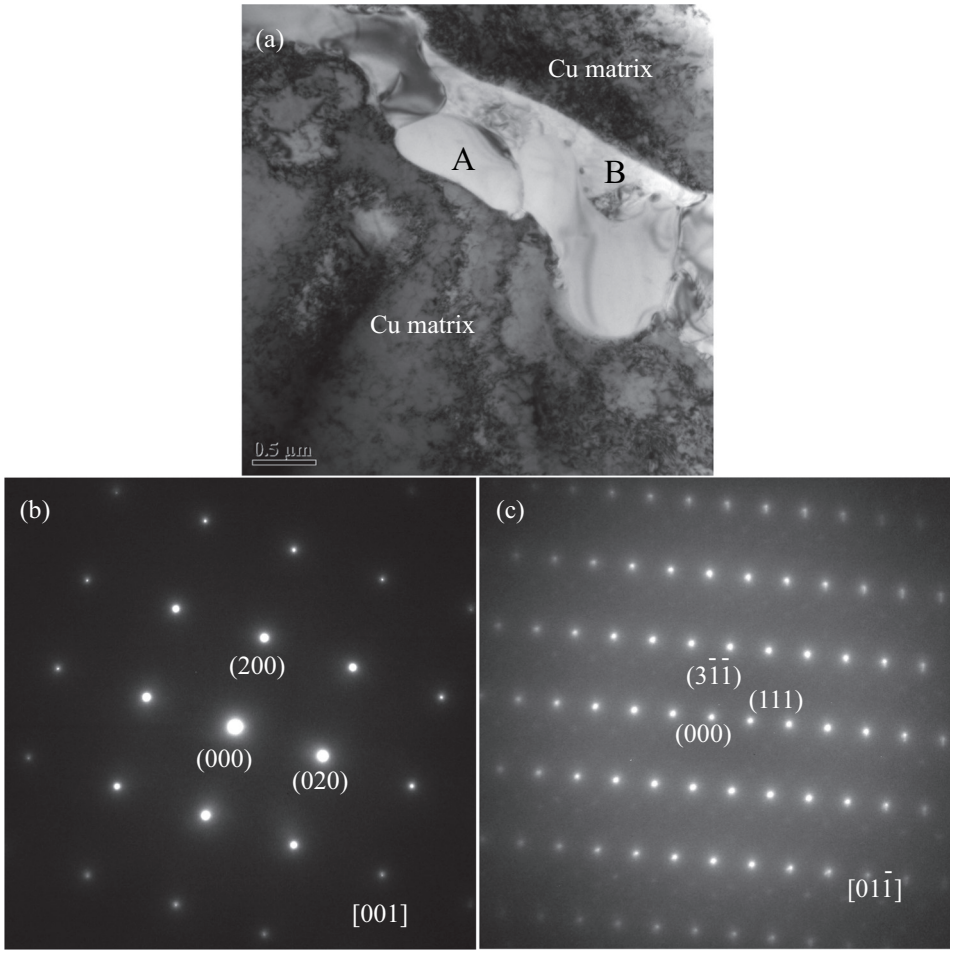

Fig. 11. TEM image and SAED patterns of TiC-Al_2O_3 coating in sample A2: (a) coating morphology, (b) TiC phase in region A, and (c) Al_2O_3 phase in region B.

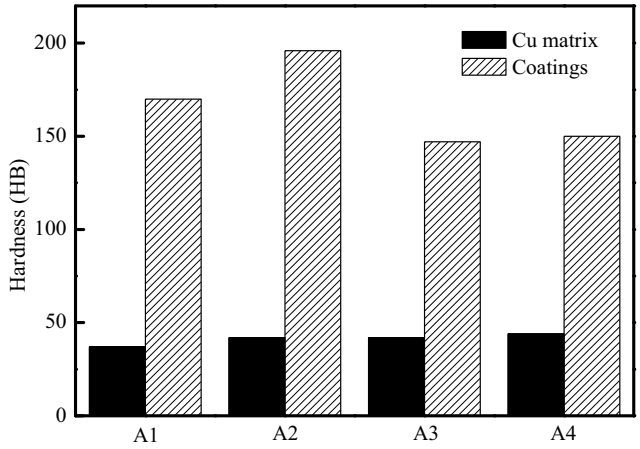

Fig. 12. Hardness values of copper matrix and strengthening coatings in samples A1-A4.

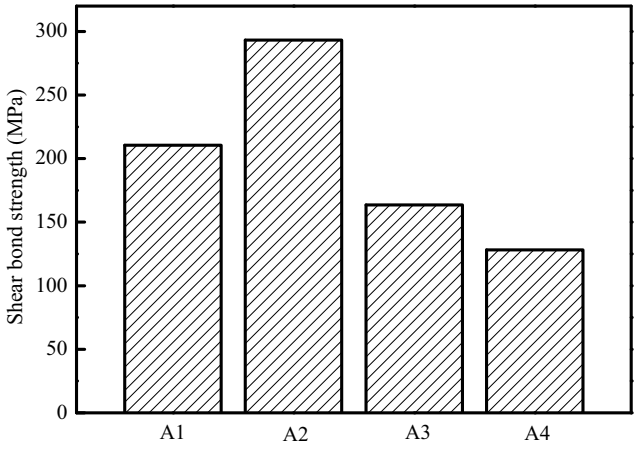

Fig. 13. Shear bond strength between composite coating and copper matrix.

20 wt% CA, the hardness reduced to 150 HB due to the poor distribution of the ceramic coating.

The shear strength tests were carried out to evaluate the bond strength, as shown in Fig. 13. Compared to sample A1, the bond strength of sample A2 increased from 210 MPa to 293 MPa. The high bond strength was credited to two things. First, fine and in-situ reinforcement particles were beneficial to improve the bond strength. Then, molten copper infiltrated into the coating, causing metallurgical bonding between the coating and the matrix. Upon further increasing the CA content, the bond strength decreased. When the CA content wasn't enough, the combustion rate of the SHS reaction was relatively

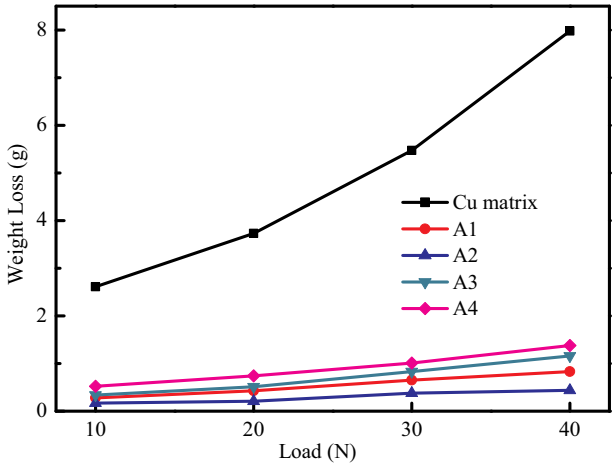

Fig. 14. Weight loss of copper matrix and composite coatings obtained from the wear test.

low. At this point, the whole temperature of the composite coating was much lower at an instant, with less molten copper infiltrating into the coating. Consequently, part of the TiC or Al_2O_3 particles adhered together. Similarly, when adding excessive CA content, the amount of outgassing significantly enhanced, giving rise to the detachment of coating by molten copper. The uniformity of the coating became worse, as shown in Fig. 9.

The wear resistance also significantly improved with in-situ TiC-Al_2O_3 composite coating synthesized on the copper matrix, as shown in Fig. 14. All four samples show better wear resistance as compared to the copper matrix. The sample A2 with 10 wt% CA content had the best resistance, and the sample A1 took the second place. With increasing load, the weight loss increased. At 40 N, the weight loss of the sample A2 was about 0.44 g, far lower than that of copper matrix (7.98 g). The enhanced wear resistance was due to the in-situ synthesized TiC-Al_2O_3 strengthening phase on the copper surface.

Now that the sample A2 showed the best wear resistance, the corresponding wear surfaces were compared with the copper matrix, as shown in Fig. 15. Long continuous grooves were observed in the copper matrix with obvious plastic deformation. With the increasing load, grooves became deeper and deeper, causing mass loss increase. The wear resistance of copper was poor, as proven in Fig. 15(a–d). When the TiC-Al_2O_3 strengthening coating was synthesized on the copper surface, the wear resistance significantly improved, as presented in Fig. 15(e–h).

The ploughing effect was demonstrated in the surface appearance of coated samples. As the load increased, a small amount of TiC, Al_2O_3 particles peeled off. The severity of abrasion wear was much less in the sample A2, and the results were in accordance with those presented in Fig. 14. In the sample A2, more uniform coating microstructure was obtained. Besides, the strengthening particles were fine, and the particle spacing was small. As a result, the hardness, bond strength, and wear resistance performance improved.

The above results indicated that the CA promoted the Ti—C SHS system. As reported in Ref. [24], residual C was found in the single Ti—C system or the Ti-Cu-C system with high Cu content during the copper casting process. Although the ignition of Ti—C SHS reaction can be achieved by molten copper, the speed of heat consumption was much quicker than that of the Ti—C reaction due to its high heat conductivity. When the highly exothermic CA reaction was employed in the Ti—C system, the released heat produced by the CA reaction was enough to ensure the full completion of the Ti—C reaction, as proven in Fig. 6. The “frozen” phenomenon didn't occur in the Ti-C-CA system. Consequently, the in-situ TiC-Al_2O_3 strengthening coating was formed on the copper surface, resulting in the significant enhancement of hardness and wear resistance. During the casting process, the Ti-C-CA SHS reaction was ignited by molten copper, forming the TiC-Al_2O_3 composite coating. Besides, the infiltration of molten copper into the SHS coating occurred, resulting in coating densification and obtaining metallurgically bonded coatings. Therefore, the bond strength between the matrix and the coating reached up to 293 MPa.

4. Conclusions

Using VEPC coupled with SHS, the in-situ TiC-Al_2O_3 strengthening coating was applied on the copper surface. Although Ti—C SHS system can be ignited by molten copper, residual carbon was found due to its incomplete reaction. Therefore, the CuO-Al (CA) system acting as a promoter was added in the Ti—C system. As a result, the in-situ TiC-Al_2O_3 composite coating was obtained during the copper casting. Besides, molten copper infiltrated into the coating, resulting in the dense coating microstructure. The optimal CA content was 10 wt%. The distribution of TiC and Al_2O_3 particles was relatively uniform. A hardness value enhancement of 388% was obtained, from 40 HB to 195 HB. And, the reduce of mass loss was significant, from 7.98 g to 0.44 g at 40 N normal wear load. Relatively high bond strength of 293 MPa was achieved. Therefore, a promising method was proposed to apply in-situ surface coating on copper with better wear resistance and higher hardness.

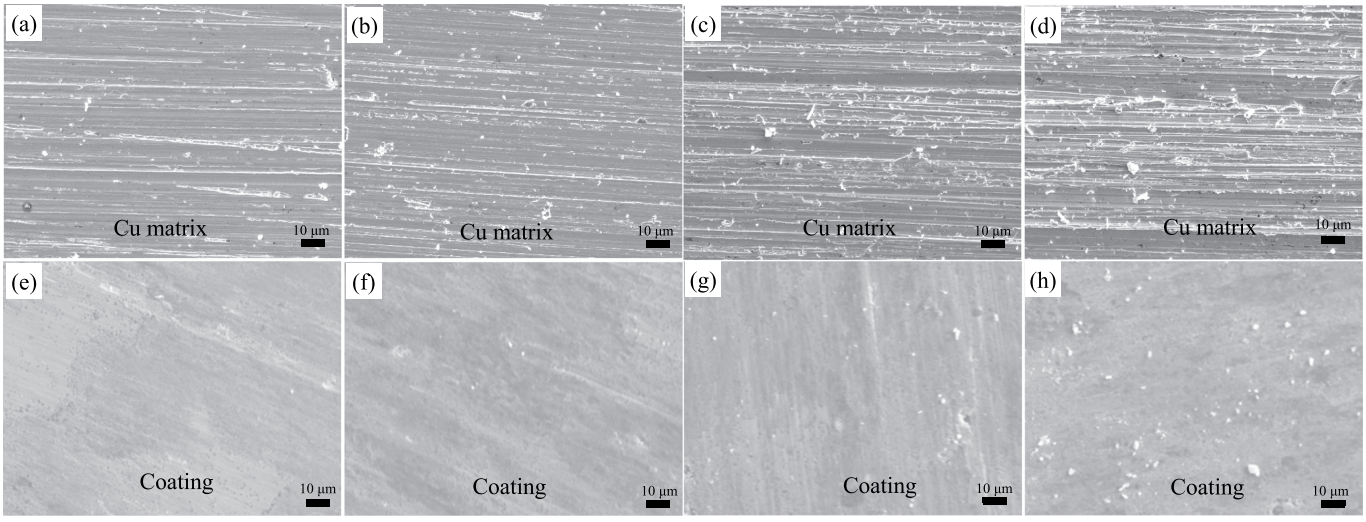

Fig. 15. SEM images of worn surface in Cu matrix and sample A2 at (a) 10 N, (b) 20 N, (c) 30 N, and (d) 40 N.

Acknowledgments

This study was funded by the China Postdoctoral Science Foundation (No. 2018M641188), the Fundamental Research Funds for the Central Universities (No. FRF-TP-18-025A1) and the National Key R &D Program of China (No. 2016YFB1101201).

Appendix A. Supplementary data

Supplementary data to this article can be found online at https://doi.org/10.1016/j.surfcoat.2019.05.064.

References

[1] K. Maki, Y. Ito, H. Matsunaga, H. Mori, Solid-solution copper alloy with high strength and high electrical conductivity, Scr. Mater. 68 (2013) 777–780, https://doi.org/10.1016/j.scriptamat.2012.12.027.
[2] Z.Y. Shi, D.Q. Wang, Z.M. Ding, Surface strengthening pure copper by Ni-B coating, Appl. Surf. Sci. 221 (2004) 62–68, https://doi.org/10.1016/S0169-4332(03)00753-0.
[3] M.X. Guo, M.P. Wang, K. Shen, L.F. Cao, Z. Li, Z. Zhang, Synthesis of nano TiB_2 particles in copper matrix by in situ reaction of double-beam melts, J. Alloy. Compd. 460 (2008) 585–589, https://doi.org/10.1016/j.jallcom.2007.06.026.
[4] G.R. Yang, Y. Hao, W.M. Song, Y. Ma, An investigation of the structure and properties of infiltrated layer on the surface of copper alloy, Mat. Sci. Eng. A 399 (2005) 206–215, https://doi.org/10.1016/j.msea.2005.03.106.
[5] J.J. Ni, J. Li, W. Luo, Q. Han, Y.B. Yin, Z.F. Jia, B.X. Huang, C.C. Hu, Z.L. Xu, Microstructure and properties of in-situ TiC reinforced copper nanocomposites fabricated via long-term ball milling and hot pressing, J. Alloy. Compd. 755 (2018) 24–28, https://doi.org/10.1016/j.jallcom.2018.04.327.
[6] D.M. Jarzabek, M. Milczarek, T. Wojciechowski, C. Dziekonski, M. Chmielewski, The effect of metal coatings on the interfacial bonding strength of ceramics to copper in sintered Cu-SiC composites, Ceram. Int. 43 (2017) 5283–5291, https://doi.org/10.1016/j.ceramint.2017.01.056.
[7] M.R. Bateni, F. Ashrafizadeh, J.A. Szpunar, R.A.L. Drew, Improving the tribological behavior of copper through novel Ti-Cu intermetallic coatings, Wear 253 (2002) 626–639, https://doi.org/10.1016/S0043-1648(02)00143-6.
[8] X.Y. Zhou, D.Q. Yi, L. Nyborg, Z. Hu, J. Huang, Y. Cao, Influence of Ag addition on the microstructure and properties of copper-alumina composites prepared by internal oxidation, J. Alloy. Compd. 722 (2017) 962–969, https://doi.org/10.1016/j.jallcom.2017.06.176.
[9] K.H. Lau, A. Sanjurjo, B.J. Wood, Aluminum and alumina coatings on copper by chemical vapor deposition in fluidized bed reactors, Surf. Coat. Technol. 54-55 (1992) 234–240, https://doi.org/10.1016/S0257-8972(09)90056-1.
[10] Y. Liu, S.Y. Li, J.J. Zhang, J.A. Liu, Z.W. Han, L.Q. Ren, Corrosion inhibition of biomimetic super-hydrophobic electrodeposition coatings on copper substrate, Corros. Sci. 94 (2015) 190–196, https://doi.org/10.1016/j.corsci.2015.02.009.
[11] J. Piotr, Z.S. Marta, C. Sebastien, P.L. Jean, Improving Fe_3Al alloy resistance against high temperature oxidation by pack cementation process, Appl. Surf. Sci. 253 (2007) 4928–4934, https://doi.org/10.1016/j.apsusc.2006.10.072.
[12] V.V. Sobolev, J.M. Guilemany, J.A. Calero, Heat transfer during the formation of an HVOF sprayed WC-Co coating on a copper substrate, J. Mater. Process. Technol. 96 (1999) 1–8, https://doi.org/10.1016/S0924-0136(99)00255-1.
[13] H. Yan, A. Wang, K. Xu, W. Wang, Z. Huang, Microstructure and interfacial evaluation of Co-based alloy coating on copper by pulsed Nd:YAG multilayer laser cladding, J. Alloys Compd. 505 (2010) 645–653, https://doi.org/10.1016/j.jallcom.2010.06.099.
[14] S. Rathod, O.P. Modi, B.K. Prasad, A. Chrysanthou, D. Vallauri, V.P. Deshmukh, A.K. Shah, Cast in situ Cu-TiC composites: synthesis by SHS route and characterization, Mat. Sci. Eng. A 502 (2009) 91–98, https://doi.org/10.1016/j.msea.2008.10.002.
[15] M. Lopacinski, J. Puszynski, J. Lis, Synthesis of ternary titanjum aluminum carbides using self-propagating high-temperature synthesis technique, J. Am. Ceram. Soc. 84 (2001) 3051–3053, https://doi.org/10.1111/j.1151-2916.2001.tb01138.x.
[16] V.V. Kurbatkina, E.I. Patsera, E.A. Levashov, A.N. Timofeev, Self-propagating high temperature synthesis of single-phase binary tantalum-hafnium carbide (Ta,Hf)C and its consolidation by hot pressing and spark plasma sintering, Ceram. Int. 44 (2018) 4320–4329, https://doi.org/10.1016/j.ceramint.2017.12.024.
[17] S. Mohammadkhani, E. Jajarmi, H. Nasiri, J. Vahdati-Khaki, M. Haddad-Sabzevar, Applying FeAl coating on the low carbon steel substrate through self-propagation high temperature synthesis (SHS) process, Surf. Coat. Tech. 286 (2016) 383–387, https://doi.org/10.1016/j.surfcoat.2015.12.029.
[18] M.A. Lagos, I. Agote, G. Atxaga, O. Adarraga, L. Pambaguian, Fabrication and characterization of titanium matrix composites obtained using a combination of self propagating high temperature synthesis and spark plasma sintering, Mat. Sci. Eng. A 655 (2016) 44–49, https://doi.org/10.1016/j.msea.2015.12.050.
[19] M. Rezaeezadeh, M.S. Afarani, M. Sharifitabar, WC-TiC-Al_2O_3 composite powder preparation by self-propagating high-temperature synthesis route, Ceram. Int. 43 (2017) 15685–15693, https://doi.org/10.1016/j.ceramint.2017.08.128.
[20] J.C. Han, X.H. Zhang, J.V. Wood, In-situ combustion synthesis and densification of TiC-xNi cermets, Mat. Sci. Eng. A 280 (2000) 328–333, https://doi.org/10.1016/S0921-5093(99)00606-1.
[21] W.M. Jiang, Z.T. Fan, D.J. Liu, D.F. Liao, X.P. Dong, X.M. Zong, Correlation of microstructure with mechanical properties and fracture behavior of A356-T6 aluminum alloy fabricated by expendable pattern shell casting with vacuum and low-pressure, gravity casting and lost foam casting, Mat. Sci. Eng. A 560 (2013) 396–403, https://doi.org/10.1016/j.msea.2012.09.084.
[22] W.M. Jiang, Z.T. Fan, D.F. Liao, D.J. Liu, Z. Zhao, X.P. Dong, Investigation of microstructures and mechanical properties A356 aluminum alloy produced by expendable pattern shell casting process with vacuum and low pressure, Mater. Des. 32 (2011) 926–934, https://doi.org/10.1016/j.matdes.2010.08.015.
[23] M. Khodai, N. Parvin, Pressure measurement and some observation in lost foam casting, J. Mater. Process. Tech. 206 (2008) 1–6, https://doi.org/10.1016/j.jmatprotec.2007.11.309.
[24] T. Shi, L.C. Guo, J.J. Hao, C.G. Chen, J. Luo, Z.M. Guo, Microstructure and wear resistance of in-situ TiC surface composite coating on copper matrix synthesized by SHS and vacuum-expendable pattern casting, Surf. Coat. Tech. 324 (2017) 288–297, https://doi.org/10.1016/j.surfcoat.2017.05.080.
[25] A. Saidi, A. Crysanthou, J.V. Wood, Characteristics of the combustion synthesis of TiC and Fe-TiC composites, J. Mater. Sci. 29 (1994) 4993–4998 https://link.springer.com/article/10.1007/BF01151089.
[26] L. Glavier, G. Taton, J.M. Ducere, V. Baijot, Stephane Pinon, T. Calais, A. Esteve, M. D. Rouhani, C. Rossi, Nanoenergetics as pressure generator for nontoxic impact primers: comparison of Al/Bi_2O_3, Al/CuO, Al/MoO_3 nanothermites and Al/PTFE, Combust. Flame 162 (2015) 1813–1820. doi:https://doi.org/10.1016/j.combustflame.2014.12.002.
[27] J.L. Lin, High rate reactive sputtering of Al_2O_3 coating by HiPIMS, Surf. Coat. Tech. 357 (2019) 402–411, https://doi.org/10.1016/j.surfcoat.2018.10.024.
[28] X. He, P. Song, X. Yu, C. Li, T.H. Huang, Y. Zhou, Q.L. Li, K.Y. Lu, J.G. Lu, J.S. Lu, Evolution of cracks within an Al2O3-40wt.%TiO2/NiCoCrAl gradient coating, Ceram. Int. 44 (2018) 20798–20807, https://doi.org/10.1016/j.ceramint.2018.08.081.
[29] A.G. Merzhanov, S.Y. Sharivker, Self-Propagating High-Temperature Synthesis of Carbides, Nitrides, and Borides, VCH, New York, 1990.
[30] M.S. Song, B. Huang, M.X. Zhang, J.G. Li, Study of formation behavior of TiC ceramic obtained by self-propagating high-temperature synthesis from Al-Ti-C elemental powders, Int. J. Refract. Met. Hard Mater. 27 (2009) 584–589, https://doi.org/10.1016/j.ijrmhm.2008.09.009.
[31] D.L. Ye, Handbook of Thermodynamic Data for Inorgainc Material, Metallurgical Industry Press, Beijing, 2002.